RSC Pharmaceutics

ROYAL SOCIETY OF CHEMISTRY

PAPER

View Article Online
View Journal | View Issue

Cite this: *RSC Pharm.*, 2025, **2**, 1545

Lactoferrin-conjugated quercetin-loaded organically modified silica nanocargoes ameliorate cognitive impairment in a rat model of amnesia

Peta Nobel Reddy,[a] Jasleen Kaur[a] and Saba Naqvi *[a,b]

Quercetin, a naturally occurring flavonoid, exerts potential pharmacological and therapeutic effects, primarily due to its antioxidant properties and ability to mitigate cognitive impairment. However, its inadequate bioavailability, poor absorption, and rapid clearance limit its therapeutic efficacy. To overcome these limitations, we developed organically modified silica (ORMOSIL) nanoparticles conjugated with lactoferrin (LF), a glycoprotein renowned for its ability to cross the blood–brain barrier and exert neuroprotective effects. This scaffold aims to enhance quercetin delivery to the brain, ultimately improving therapeutic outcomes. This study employed a multi-faceted approach, involving the detailed characterization of nanoparticles, and *in vivo* assessment using a rat model to evaluate cognitive functions after scopolamine-induced amnesia. Behavioral tests, biochemical assessment, potential to inhibit the acetylcholinesterase enzyme, and histological findings collectively indicate improved efficacy of LF-Q-ORMOSIL compared to quercetin and ORMOSIL alone in an acute study. Furthermore, *in vivo* and *ex vivo* biodistribution patterns suggest better retention and increased brain targeting of the LF-conjugated formulation in the brain. Our findings demonstrate that LF-Q-ORMOSIL holds promise for enhanced delivery and therapeutic efficacy in mitigating cognitive deficits associated with neurodegenerative processes.

Received 7th April 2025,
Accepted 19th August 2025

DOI: 10.1039/d5pm00093a

rsc.li/RSCPharma

Introduction

Alzheimer's disease (AD) is a chronic neurological condition that causes memory loss over time. It is characterized by oxidative stress in the brain and loss of cholinergic neurons in the hippocampus and basal forebrain. The central cholinergic neuronal activity is crucial for memory and learning. In the creation of memories, numerous neurotransmitters and neural pathways are involved. Cognitive impairments seen in AD are linked to functional cholinergic system abnormalities.[1] According to the Alzheimer's and Related Disorders Society of India's "Dementia India" study, with an estimated 4.1 million cases worldwide, India has the second-highest population of dementia patients. By 2035, this is anticipated to quadruple. By 2030, there will be 7.3 million Alzheimer's patients in India, up from the present four million.[2]

Animal experiments show that the muscarinic cholinergic receptor antagonist scopolamine exerts significant amnestic effects. The experimental animal model of scopolamine-induced amnesia has been frequently used to investigate novel compounds and formulations with potential therapeutic benefits in dementia. It disrupts the transmission of acetylcholine in the central nervous system, causing cholinergic dysfunction and memory deficits in rats.[3,4]

In the human diet, quercetin is a well-known flavonoid that is found in foods including onions, red wine,[5] ginkgo biloba, edible fruits, and vegetables. One of the well-known dietary antioxidants, quercetin, exhibits biological benefits that include defence against some types of cancer,[6] inflammation and cardiovascular disorders.[7] Despite these health advantages, the clinical use of quercetin is severely constrained due to its low bioavailability (less than 17% in rats and even 1% in humans),[8] which is caused by its poor water solubility. Developing a technology that could make quercetin more soluble is therefore necessary. A new opportunity for drug administration is provided by nanotechnology. Advances in nanomedicine have made the development of carrier systems that can transport medications to target areas by focusing on a specific component of the cell surface possible. To transport medications to a specific place, a variety of nanoparticles, including inorganic, liposomal, polymeric, albumin, and others, have been produced. Due to their inert nature,

[a]*Department of Pharmacology and Toxicology, National Institute of Pharmaceutical Education and Research (NIPER-R), Bijnor-Sisendi Road, P.O. Mati, Lucknow, UP–226002, India*
[b]*Regulatory Toxicology, National Institute of Pharmaceutical Education and Research (NIPER-R), Bijnor-Sisendi Road, P.O. Mati, Lucknow, UP–226002, India*

silica nanoparticles are among the most adaptable types of nanoparticles. They also assist as target delivery carriers for biological entities such as enzymes, drugs, and genetic material. It offers various binding sites for molecules to have affinity towards its surface, functionalized with hydroxyl, thiol, amino, and carboxyl groups to act as target drug delivery vehicles.[9]

Lactoferrin (LF), a glycoprotein having a positive charge for binding to iron, is one of the most attractive potential targets because of its low cost, strong receptor-mediated transport activity and improved biocompatibility.[10] LF receptors can facilitate LF-mediated transcytosis through *in vitro* BBB because they are present in human VECs of the BBB.[11–13] Exogenous LF may readily cross the blood–brain barrier (BBB) and reach neural tissues since lactoferrin receptors (LFRs) are present on brain capillary endothelial cells and neurons. As a result, LF has been successfully employed as a brain-targeting ligand in drug delivery systems, enabling enhanced transport of therapeutics across the blood–brain barrier *via* receptor-mediated uptake.[12,14–17]

Herein, we employed a multi-faceted approach, including synthesis, thorough characterization, and *in vivo* assessments of LF conjugated ORMOSIL nanoparticles. It involves characterizing the nanoparticles for size, zeta potential, and drug release profile. In *in vivo* experiments, a rat model to evaluate the cognitive function post-scopolamine administration was employed, with and without treatment with the nanoparticle formulation. Behavioural tests were utilized to assess memory and learning. Biochemical assays measured oxidative stress markers and cholinesterase activity in brain tissues.

Our findings demonstrate that lactoferrin-conjugated quercetin-loaded ORMOSIL nanoparticles significantly improved cognitive performance and reduced oxidative stress and cholinesterase activity compared to the scopolamine-induced group as well as quercetin-administered animals. This suggests that these nanoparticles hold promise as a therapeutic strategy for preventing or mitigating cognitive deficits associated with neurodegenerative diseases like Alzheimer's.

Materials and methods

Materials

Scopolamine, lactoferrin (LF), donepezil, *N*-hydroxy succinimide (NHS), and 1-ethyl-3-(3-dimethylaminopropyl) carbodiimide (EDC) were purchased from Sigma Aldrich Chemicals (USA). All other chemicals used in this study were of analytical reagent grade and were purchased from Himedia and Merck.

Methods

Synthesis of quercetin-loaded QRMOSIL (Q-ORMOSIL) nanoparticles. A Tween 80/1-butanol/water micelle nonpolar core was used to create nanoparticles. Briefly, ORMOSIL nanoparticles were made by dissolving Tween 80 and *n*-butanol in double-distilled water and swirling magnetically at 600 rpm for 5 min. A transparent solution was prepared by dissolving 2 mg of quercetin in 50 μL of dimethylformamide (DMF), which was then added to the mixture above while being continuously stirred at 600 rpm. For the void nanoparticle preparation, quercetin was replaced with 50 μL of DMF alone. The solution was mixed with triethoxyvinylsilane for an hour until the mixture became transparent. The system was then filled with 3-aminopropyltriethoxysilane and agitated with a magnetic stirrer for 48 hours. The reaction was carried out at room temperature. To eliminate unreacted free molecules from the reaction mixture, the synthesized nanoparticles were dialyzed for two days using a dialysis membrane (12 kDa cutoff, Sigma). The completed product was lyophilized and kept at 4 °C for later use.[18]

Synthesis of lactoferrin conjugated quercetin loaded QRMOSIL nanoparticles (LF-Q-ORMOSIL). The synthesized nanoparticles were added to the prepared solution together with equal volumes of NHS and EDC and agitated for one hour. After that, 600 μL of bis-carboxy-polyethylene glycol (PEG) at a concentration of 100 μg mL^{-1} was added and agitated at 4 °C overnight. Again, equal concentrations of NHS and EDC were added to the above solution. Thereafter, 70 μg of lactoferrin was added to start the reaction after stirring for approximately 30 minutes. The reaction was carried out overnight on ice. To eliminate unreacted free molecules from the reaction mixture, the synthesized nanoparticles were dialyzed for two days using a dialysis membrane (12 kDa cutoff, Sigma). The completed product was lyophilized and kept at 4 °C for later use. The schematic illustration is given in Fig. 1.[10]

Physical characterization of nanoparticles

Dynamic light scattering (DLS). The mean particle size, polydispersity index (PDI), and zeta potential of the ORMOSIL and LF conjugated nanoparticles were determined using dynamic light scattering (DLS) with a zeta sizer (Malvern Co., UK). Throughout the experiment, measurements were made using a glass cuvette while maintaining a temperature of 25 °C. Triple-distilled water was used to dilute the prepared nanoparticles before they were measured with a Zeta sizer.

UV/vis spectrophotometer. UV-visible spectrophotometry was performed using an Agilent Cary UV spectrophotometer, USA. The purpose of the procedure was to identify quercetin's and ORMOSIL's distinctive absorption peaks over a range of 200–800 nm.

Fourier transform infrared (FTIR) spectroscopy. FTIR (ALPHA, BRUKER, Germany) was carried out to determine the different functional groups present in the synthesized formulation. FTIR spectra of Q-ORMOSIL, quercetin, and LF Q-ORMOSIL nanoparticles were recorded in the spectral range of 4000–500 cm^{-1}.

Scanning electron microscopy and EDS analysis. A scanning electron microscope (JEOL, Model: JSM-IT-200) was used to obtain the surface morphology of nanoparticles. It is also possible for the SEM to analyse specific point locations on the sample; this method is particularly helpful for figuring out chemical compositions (using EDS) in a qualitative or semi-quantitative manner.

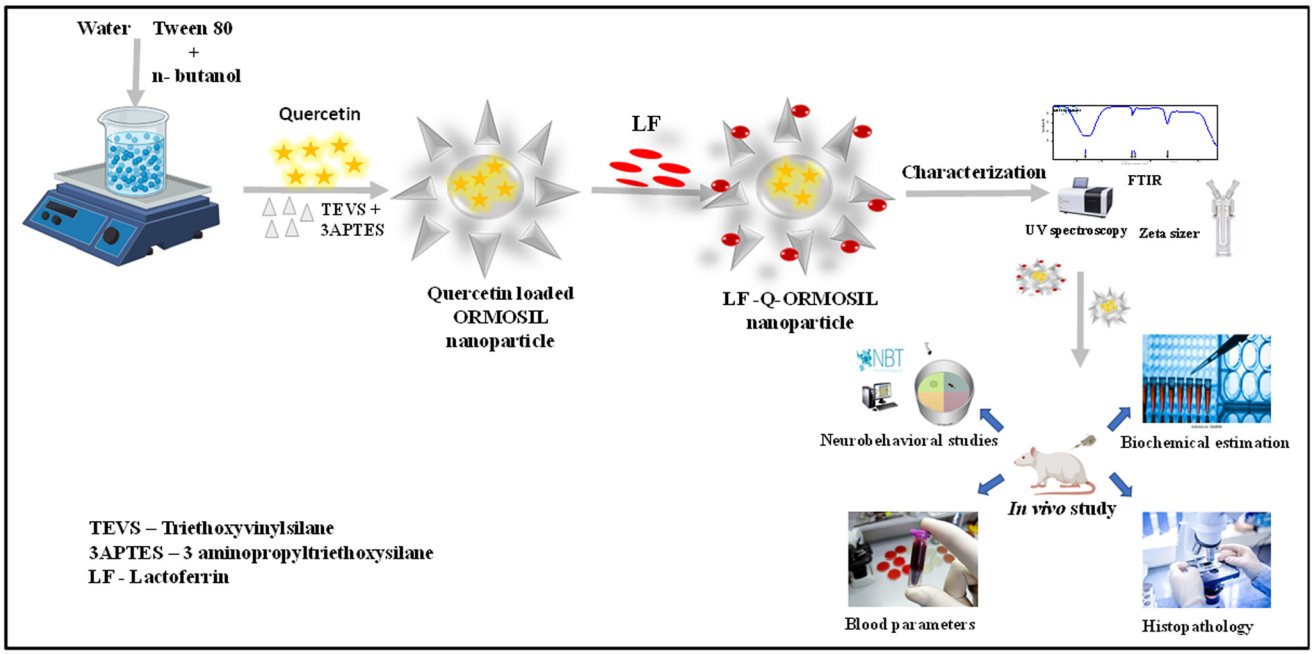

Fig. 1 Schematic illustration of LF-Q-ORMOSIL synthesis, characterization, and *in vivo* assessment.

Transmission electron microscopy (TEM). TEM was used to analyse the size and shape of the synthesized nanoparticles (Talos L120C TEM) at Jamia Hamdard, New Delhi. The transmission electron microscope (TEM) instrument was optimized to achieve an extremely higher magnification and resolution than SEM. TEM provides important insight into a sample's internal structure, such as its crystal structure, morphology (particles, grains, *etc.*), topography (structure, shape, *etc.*) and composition (elemental mapping).

Entrapment efficiency (EE%). Quercetin loading was determined by calculating the entrapment efficiency (%), which was evaluated by taking 2 ml of synthesized nanoparticles and centrifuging them at 6000 rpm for 15 minutes. After that, the supernatant was collected and the absorbance was measured at 368 nm, and then the free drug concentration was calculated by using the standard curve equation of quercetin.

The entrapment efficiency was calculated as follows:

$$\text{Entrapment efficiency}\,(E\%) = \frac{\text{total drug} - \text{free drug (unentrapped drug)}}{\text{total drug}} \times 100$$

***In vitro* quercetin release study.** The synthesized nanoparticles were introduced into a membrane dialysis bag (12 kDa cutoff). The dialysis bag was then placed in 100 ml of phosphate buffer (pH 7.4) which was used as release medium and maintained at 37 °C with constant stirring at 100 rpm. 1 ml sample aliquots of the medium were collected from all the samples at a particular interval of time (0, 0.25, 0.5, 0.75, 1, 2, 4, 8, 12, 24, 48, 72, and 96 h) and then the medium was replaced with the same volume of fresh release medium. All the samples were analysed by using UV-visible spectroscopy at a wavelength of 368 nm. The validated UV-visible spectroscopy method was used to determine the drug concentration at a particular interval of time. The average values were determined, and a time-*versus*-cumulative-percentage plot was created using the results.

***In vivo* imaging and biodistribution analysis.** ICG loaded ORMOSIL nanoparticles were prepared the same way as the above ORMOSIL nanoparticle synthesis process, but here we used ICG, which was dissolved in water (1 mg ml^{-1}) instead of the drug quercetin. After preparation, both free ICG and the nanoparticles were injected into the rats *via* the i.p. route. Fluorescence images of free ICG and ICG-loaded nanoparticles were acquired at 0, 1, 3, 6, 12, and 24 h after injection using a Perkin IVIS with a 745 nm excitation wavelength and an 820 nm filter to collect FL signals of ICG and ICG conjugated nanoparticles. The rats, after injection at 24 h, were sacrificed, and the brain, along with other organs, including heart, liver, spleen, lungs, kidneys, and testes, was collected for imaging and semiquantitative biodistribution analysis.

Animals. The experiment was performed using male Wistar rats weighing 150–180 g, procured from the Animal House Facility of CSIR-IITR, Lucknow. The experimental protocol was duly approved by the Institutional Animal Ethics Committee (IAEC), NIPER-Raebareli. The care of the animals was carried out as per the guidelines of the Committee for Control and Supervision of Experiments on Animals (CCSEA). All animals were kept in animal cages and were maintained at a constant temperature with a 12 h light/12 h dark cycle, air conditioning, a temperature range of 20–22 °C and a humidity of 45–55%.

Experimental design. The animals were treated with the following regimen for 14 days after being split up into 6 groups of 5 animals each, as shown in Fig. 2.

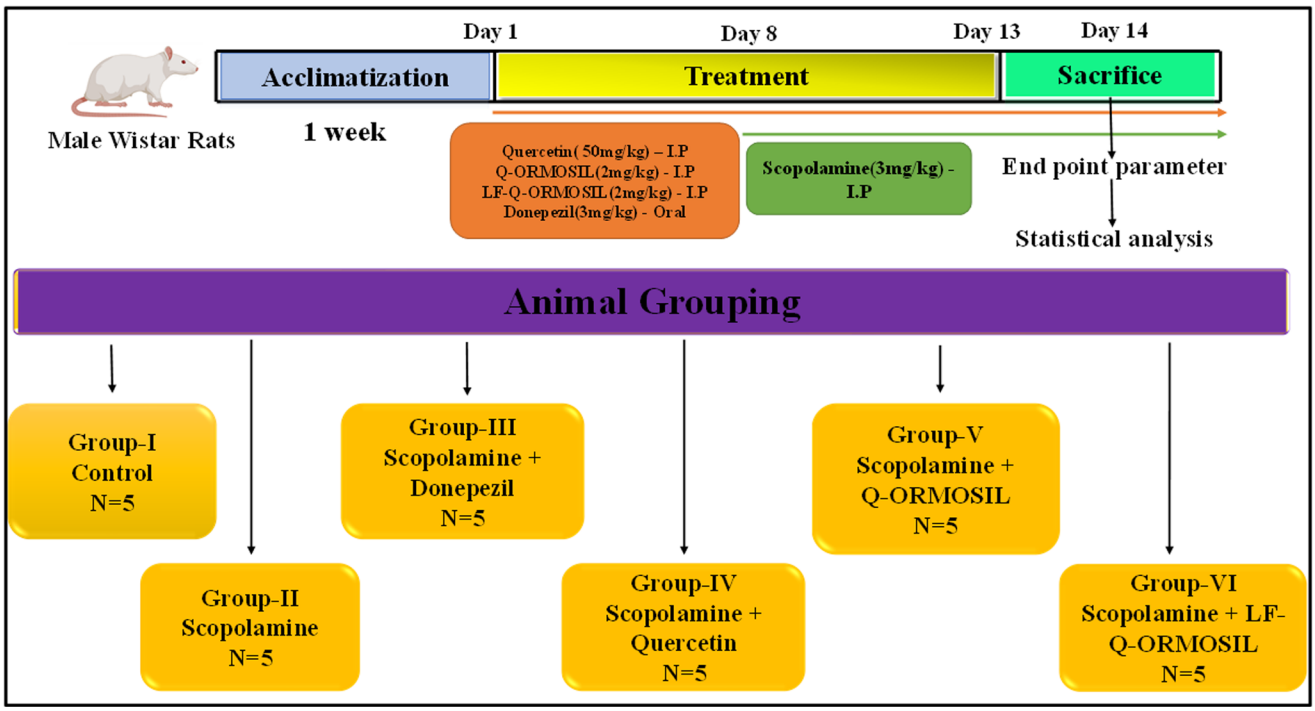

Fig. 2 Experimental design for *in vivo* assessment of LF-Q-ORMOSIL.

Group 1 – Normal saline (0.9% NaCl) (control);

Group 2 – Scopolamine (3 mg kg^{-1}, intraperitoneally); (SCO)

Group 3 – SCO (3 mg kg^{-1} i.p.) + donepezil (3 mg kg^{-1} p.o.); (SCO + D)

Group 4 – SCO (3 mg kg^{-1} i.p.) + quercetin (50 mg kg^{-1} i.p.); (SCO + Q)

Group 5 – SCO (3 mg kg^{-1} i.p.) + Q-ORMOSIL NPs (2 mg kg^{-1} i.p.); (SCO + Q-ORMOSIL)

Group 6 – SCO (3 mg kg^{-1} i.p.) + LF-Q-ORMOSIL NPs (2 mg kg^{-1} i.p.); (SCO + LF-Q-ORMOSIL)

Treatment drugs were given daily for 1–7 days to adapt them for the route of administration and their metabolism before behavioural tasks; treatment continued on days 8–14. Scopolamine was given intraperitoneally for 7 days (days 8–14). On days 8–14, treatment drugs and scopolamine were administered at 60 min and 30 min before training, respectively.

At the end of the study (after the last dose), animals were anesthetized with the help of urethane (5 mg kg^{-1}) by intraperitoneal injection. After that, blood (3–4 ml) was collected from the retro-orbital sinus. Blood samples were placed in non-heparinized glass tubes, where they were left to coagulate for 30 minutes at 25 °C. Centrifugation at 1000*g* for 10 min was used to separate the serum samples. These sera were stored at −80 °C and were used for biochemical analysis. After the collection of blood samples, the animals were sacrificed by cervical dislocation. The brains were excised and washed with ice-cold saline and PBS. One part was stored in 10% formalin for histopathology, while another part 10% (w/v) was homogenized with ice-cold PB buffer (pH 7.4) and utilized for biochemical estimations. The supernatants were collected as tissue homogenates and stored at −80 °C until further use.

Neurobehavioral assessments

Open field test (OFT). The locomotor and behavioral activities of the rats were evaluated using an open field activity monitoring test. A wooden device that was divided into 16 (4 × 4) squares was used to record observations. The animal was put in a corner of the room, and its behavior was recorded for five minutes. The test measured: (i) squares explored (number of line crossings) and (ii) total time spent in the center (s).[19]

Elevated plus maze (EPM) test. Rats were positioned one by one at the open arm's end. Transfer latency (TL), which was measured as the time taken by each rat to go to the closed arm, was reported to be 90 s. The animals were given unrestricted access to the equipment on the first day of the experiment for at least 10 minutes. The first-day TL shows acquisition (learning), while the last day TL defines the learning based memory retention.[2]

Morris water maze (MWM) test. The Morris water maze (MWM) test was used to assess spatial memory and learning. The apparatus consisted of a circular pool with a diameter of 150 cm and a height of 45 cm, filled with water to a depth of 30 cm, maintained at 28 °C. A small amount of milk powder was added to render the water opaque. The pool was virtually divided into four equal quadrants (Q1, Q2, Q3, and Q4) using ANYMAZE software. A hidden platform (10 cm in diameter, white, and submerged 1 cm below the water surface) was placed at the center of the fourth quadrant (Q4) and remained in this position throughout the experiment. On each training

day (day 7 and day 14), each rat underwent four consecutive trials with a 15-minute inter-trial interval. For each trial, the rat was released into the water facing the wall of the tank, with the starting position pseudo-randomly rotated among the quadrants to minimize directional bias. The maximum duration allowed for each trial was 120 seconds. If a rat failed to locate the hidden platform within this time, it was gently guided to the platform and allowed to remain there for 20 seconds to orient itself. The primary outcome measure was escape latency time (ELT), defined as the time taken by the animal to find and climb onto the platform. The ELT for each day was calculated as the average of the four trials. No probe test was performed in this study, as the focus was on acquisition learning and spatial memory during the training phase.[20]

Estimation of oxidative stress parameters

Reactive oxygen species (ROS). With some minor modifications, the protocol for ROS was carried out as given by Socci *et al.* The solution was prepared by taking a sample with phosphate buffer and vortexing. 20 μM DCFDA was added to the reaction mixture. The resulting mixture was incubated for 30 min at 37 °C. This allows the conversion of DCFDA to DCF, and after loading wells with 200 μl of each sample, the fluorescence was recorded at 485 nm excitation and 529 nm emission.[21]

Thiobarbituric acid reactive substances (TBARS). The lipid peroxidation level was determined by measuring the malondialdehyde (MDA) levels. The level of lipid peroxidation is directly related to the rise in oxidative stress and inflammation. 0.5% w/v of tissue homogenate or standard solution (tetra ethoxy propane) was incubated for 10 minutes in sodium dodecyl sulphate and then 20% acetic acid was added. Thiobarbituric acid (0.8%) and distilled water were added to the reaction mixture and vortexed. Then it was allowed to incubate for 1 h in a boiling water bath. After cooling, it was centrifuged for 10 minutes at 2000 rpm. The pink chromogen/complex developed in the supernatant was acquired, and its absorbance was measured at 532 nm.[22]

Catalase activity. The assay was performed by making modifications to the literature method.[23] The catalase level in the brain was determined by taking 100 μL of tissue homogenate with 500 μL of 0.2 M H_2O_2, 0.01 M phosphate buffer, and it was incubated for 60 s at room temperature. Acetic acid and 5% potassium dichromate were used in a 1 : 3 ratio to cease the reaction. This reaction mixture was further incubated in a water bath for 10 min, and it was cooled to acquire the absorbance at 570 nm using a multi-mode reader.

Reduced glutathione (GSH). The reduced glutathione activity was measured using a previous method[24] with some modifications. The sample was loaded along with the addition of phosphate EDTA buffer. The solution was vortexed and 750 μl of Ellmann's reagent was added, followed by incubation at 37° C in a water bath for 10 min, and the resultant mixture was cooled and plates were loaded with 300 μl of each sample and absorbance was measured at 412 nm. Reduced glutathione is used as a standard with concentrations from 5 to 320 μM.

Superoxide dismutase (SOD). Sodium pyrophosphate was added to the supernatant, and then phenazine methosulphate, nitro blue tetrazolium, nicotinamide adenine dinucleotide, and distilled water were added. The reaction mix was maintained at 30 °C for 90 seconds. Glacial acetic acid, within 1.5 minutes, was added to cease the reaction, and the violet resulting colour complex was measured at 560 nm of absorbance.[25]

Haematological parameters. Blood samples were collected in tubes containing EDTA and red blood cells (RBC), white blood Cells (WBC), haemoglobin (HGB), and haematocrit (HCT) were measured by using a Mindray (BC 5000) Auto Haematology Analyzer.

Histopathology. Rats were sacrificed, and 10% formalin was used to preserve the brain tissue. The brains were prepared, encased in paraffin wax, and sectioned into 5 μm-thick pieces using a microtome. These sections underwent processing and mounting on slides before being stained with haematoxylin and eosin and inspected under a light microscope.

Statistical analysis. The statistical data were expressed as the mean ± standard error of the mean (SEM). We used GraphPad (Prism 8) software for analysing the statistical difference by using one-way ANOVA (analysis of variance) followed by Tukey's multiple comparison tests. The level of statistical significance was set at $*p < 0.05$, $**p < 0.01$, $***p < 0.001$ and $****p < 0.0001$ *vs.* control and $\#p < 0.05$, $\#\#p < 0.01$, $\#\#\#p < 0.001$ and $\#\#\#\#p < 0.0001$ *vs.* scopolamine.

Results

Characterization of LF-Q-ORMOSIL nanoparticles

The mean particle size, polydispersity index (PDI), and zeta potential of the ORMOSIL and LF conjugated nanoparticles were determined using dynamic light scattering (DLS) with a zeta sizer (Malvern Co., UK), and the average particle size was found to be 108.8 nm and 105.9 nm for Q-ORMOSIL and LF-Q-ORMOSIL respectively and the PDI was 0.098 and 0.005 for Q-ORMOSIL and LF-Q-ORMOSIL. Zeta potentials for the two formulations were found to be 21.7 mV and 25.7 mV, respectively (Fig. 3A–D).

Upon performing UV-visible spectrophotometry, characteristic quercetin and ORMOSIL absorption peaks were observed between 200 and 800 nm. The characteristic peak for quercetin alone was observed at 410 nm, whereas quercetin and ORMOSIL nanoparticles were observed at 368 nm (Fig. 3E). The existence of surface and functional groups, as well as the functional group's interaction with the drug, was confirmed by FT-IR spectroscopy. LF surface alteration of Q-ORMOSIL was confirmed by FTIR. The primary spectral bands in the LF sample, which can also be found in the functionalized nanoparticles, are those at around 1650 and 1560 cm^{-1}, which are associated with the C═O stretching and N–H bending vibrations of the amide I and amide II functional groups of the LF protein, respectively. The amide I band of LF was

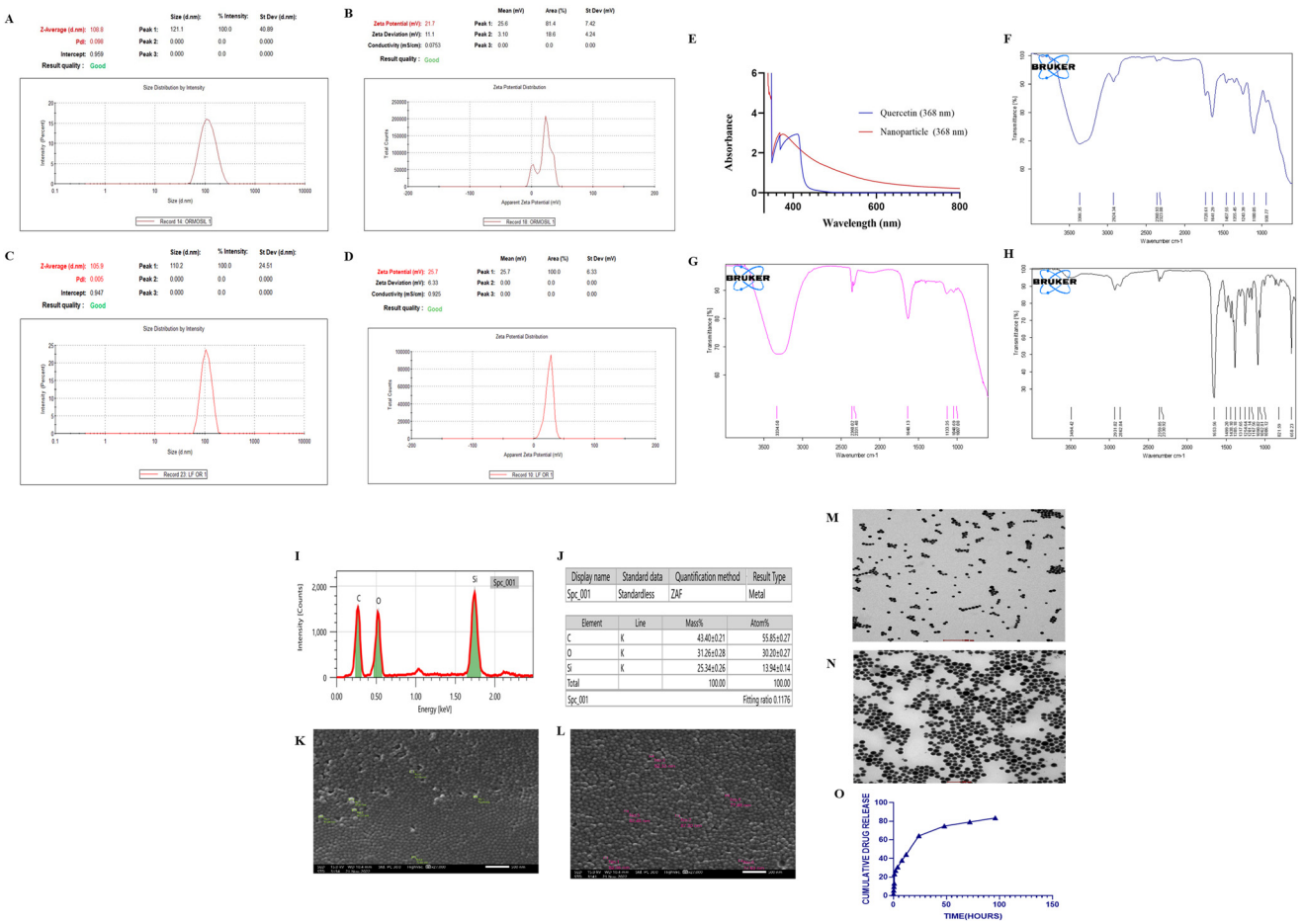

Fig. 3 Characterization of Q-ORMOSIL and LF-Q-ORMOSIL nanoparticles: (A and B) particle size distribution and zeta potential of Q-ORMOSIL nanoparticles, (C and D) particle size distribution and zeta potential of LF-Q-ORMOSIL nanoparticles, (E) UV-visible spectroscopic analysis of quercetin and quercetin loaded nanoparticles, (F–H) The FTIR spectra of LF-Q-ORMOSIL, Q-ORMOSIL, and quercetin, (I and J) representation of EDS analysis of nanoparticles, (K and L) SEM images of Q-ORMOSIL and LF-Q-ORMOSIL, respectively, (M and N) TEM images of Q-ORMOSIL and LF-Q-ORMOSIL, respectively, (O) *in vitro* quercetin release for a duration of 96 hours at 7.4 pH.

observed at 1650 cm^{-1} and underwent a shift to 1710 cm^{-1} in the functionalized NPs, whereas the amide II band changed from 1560 to 1600 cm^{-1}. These results appear to support that LF was covalently conjugated on the nanoparticle surfaces. In the interaction between ORMOSIL and LF, there was some absorption that could be seen at 3334 cm^{-1} with increasing absorption and 1640 cm^{-1} with extreme intensity, which is indicative of NH_2 vibration and the creation of N–H bonds (Fig. 3F– H).

SEM was used to measure the size of the ORMOSIL and LF coupled nanoparticles, and the results indicated that the particles were spherical, with an average size of 80 nm. Silica makes up 25% of the sample under SEM-EDS examination, which is a non-destructive analytical approach. The remaining peaks in the EDS spectrum represent the other (C and O) elements (Fig. 3I–L). Similarly, the average size was observed to be about 80 nm, with a spherical shape, and the non-aggregated morphologies of the nanoparticles observed in the TEM analysis of Q-ORMOSIL and LF-Q-ORMOSIL are shown in Fig. 3M and N. Furthermore, to find the entrapment efficiency (%), different concentrations of quercetin from 2.5, 5, 7.5, 10, 12.5, and 15 μg ml^{-1} were prepared, and their absorbance was checked at 368 nm and different concentrations and plotted as shown in Fig. 3O. As a result, the entrapment efficiency of quercetin-loaded ORMOSIL nanoparticles was found to be 89.28%.

In vivo toxicological assessment of LF-Q-ORMOSIL *via* body weight changes and hematological parameters

Fig. 4A signifies the changes in body weight patterns during the 13 days of dosing duration, in which significant body weight reduction can be observed in the scopolamine group, while those groups co-administered with scopolamine and nanoparticles retained their body weight during the experimental period. Furthermore, the effect of NPs on WBC is

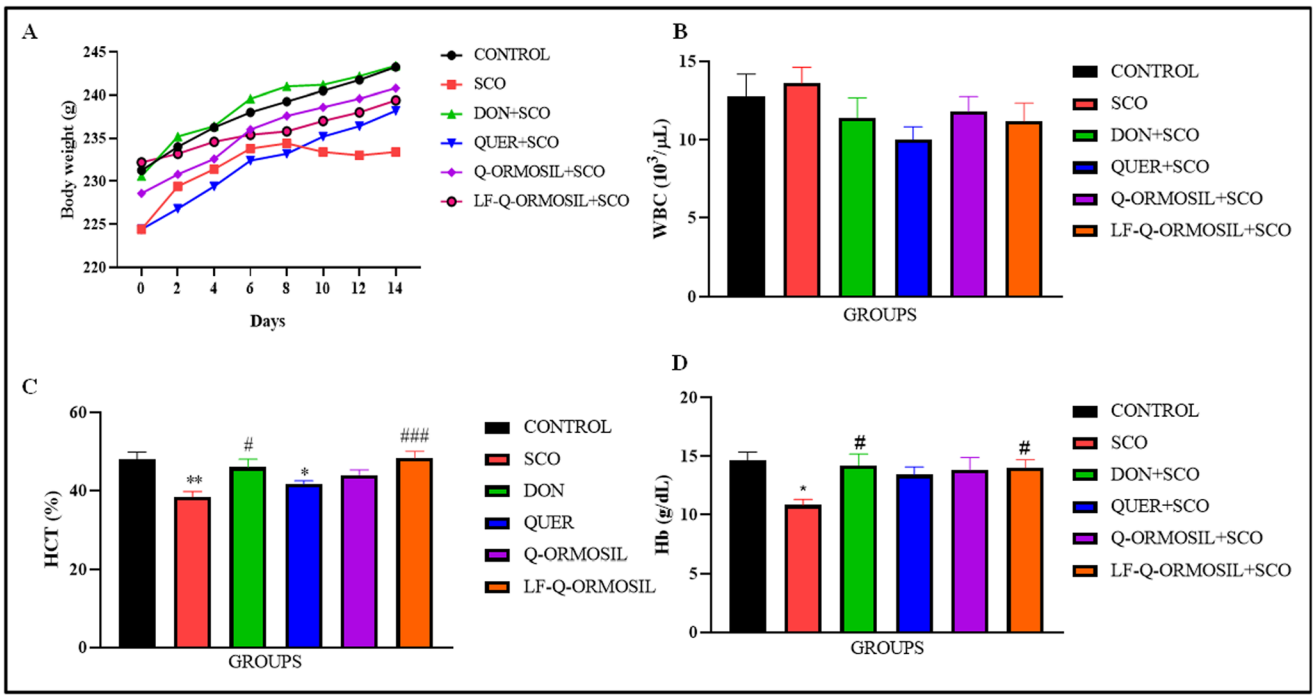

Fig. 4 *In vivo* toxicological assessment: (A) body weight changes of different groups during the dosing of 2 weeks; hematological analysis *via* changes in (B) WBCs, (C) hematocrit% (%HCT), and (D) hemoglobin (Hb g dL^{-1}). Represented as mean ± SEM. Statistical analysis is carried out by using one-way ANOVA followed by Tukey's multiple comparisons. The statistical significance was considered at *$p < 0.05$, **$p < 0.01$. *vs.* control group; #$p < 0.05$, and ##$p < 0.01$ *vs.* scopolamine group.

depicted in Fig. 4B. Scopolamine showed an increased WBC count when compared with the control. Quercetin, Q-ORMOSIL, and LF-Q-ORMOSIL groups showed decreased WBC counts when compared with scopolamine. The effects of NPs on haemoglobin (Hb) and haematocrit (HCT) are depicted in Fig. 4C and D, respectively. Scopolamine showed decreased Hb and %HCT counts when compared with the control, while quercetin, Q-ORMOSIL, and LF-Q-ORMOSIL groups showed improved Hb and %HCT counts when compared with scopolamine.

Effects of LF-Q-ORMOSIL on the alterations of neurobehavioral patterns in scopolamine-induced amnesia

In OFT, animals that received scopolamine showed a decrease in the number of line crossings, in contrast to the animals of the control group. However, animals that received LF-Q-ORMOSIL demonstrated a significant increase in the number of line crossings when compared to those that received scopolamine, significantly and even better than quercetin and ORMOSIL-treated animals, as shown in Fig. 5A. Similarly, the time spent in the center of the open field was reduced significantly in animals given scopolamine, in contrast to the control animals. However, LF-Q-ORMOSIL administered animals showed a significant increase in the time spent when compared to scopolamine-treated animals, as shown in Fig. 5B. Moreover, the study defined the transfer latency period as the amount of time it took each animal to travel from the open arm to the closed arm. According to the EPM model findings, scopolamine-treated animals showed significantly increased transfer latency when compared to control animals. In contrast, animals receiving LF-Q-ORMOSIL showed a considerable reduction in the transfer latency period when compared to animals receiving scopolamine treatment, as shown in Fig. 5C. Likewise, results of the MWM test indicate that scopolamine-treated animals significantly increased their escape latency when compared to control animals. However, the treatment groups showed a significant decrease in the latency period. Q-ORMOSIL and LF-Q-ORMOSIL treatments significantly decreased the latency period, as shown in Fig. 5D. When compared to the control group, the scopolamine group's time spent in the target region was dramatically reduced. Compared to the scopolamine group, pre-treatment groups showed significantly more time spent in the target quadrant, as shown in Fig. 5E.

Assessment of LF-Q-ORMOSIL for its anti-oxidant activity and potential to inhibit acetylcholinesterase activity

Scopolamine showed increased TBARS levels when compared with the control. However, animals that received bulk quercetin, Q-ORMOSIL, and LF-Q-ORMOSIL showed decreased TBARS levels when compared with scopolamine. In comparison with quercetin alone and Q-ORMOSIL, the group treated with LF-Q-ORMOSIL showed a substantial change in the levels of TBARS (Fig. 6A). Similarly, the effect of nanoparticles on

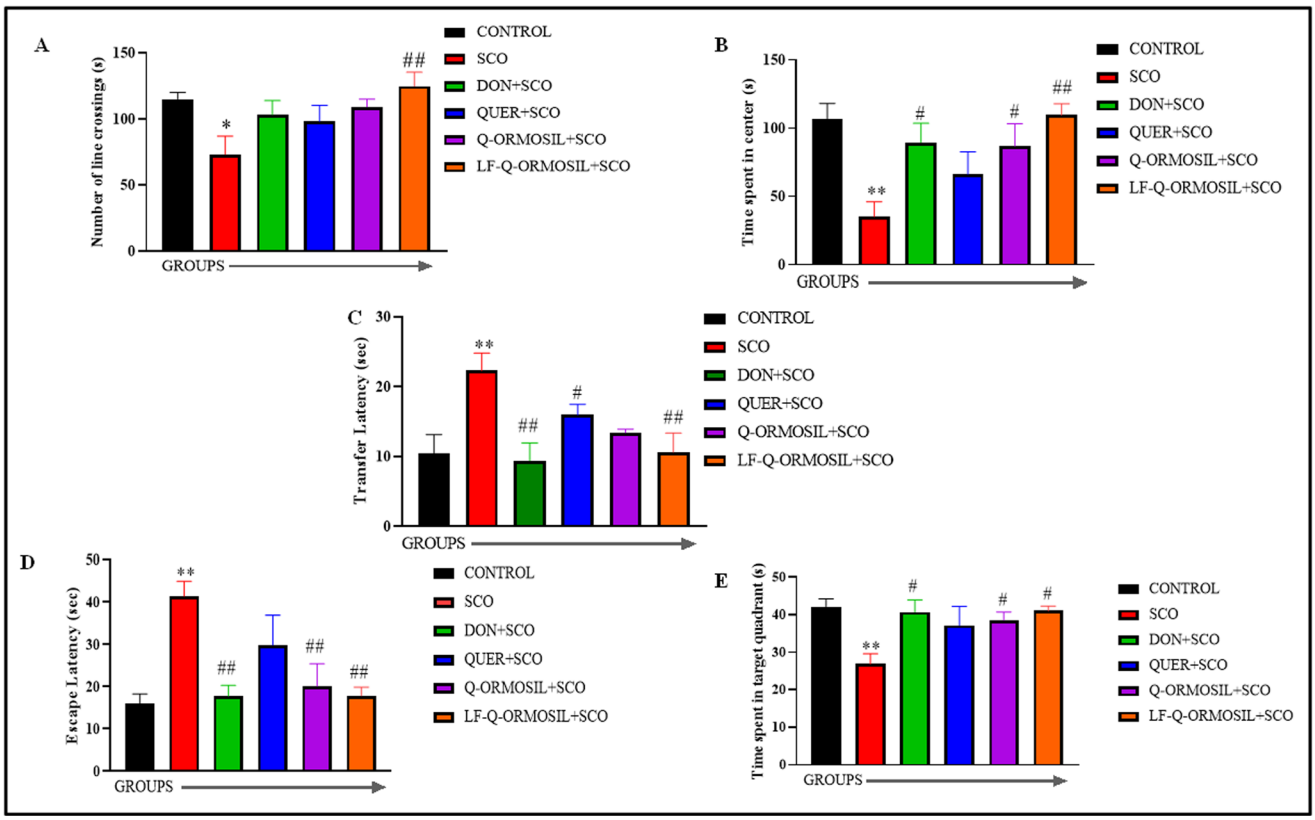

Fig. 5 Neurobehavioral assessment of different groups: effect of NPs on the open field test (OFT): (A) number of line crossings and (B) time spent in the center; effect of NPs on the elevated plus maze test: (C) transfer latency; on the Morris water maze test: (D) escape latency and (E) time spent in target quadrant. All the data was expressed as mean ± SEM (N = 5). One-way ANOVA was used in the statistical analysis, followed by Tukey's multiple comparison tests. The statistical significance was considered at *p < 0.05, **p < 0.01, ***p < 0.001 *vs.* control; #p < 0.05, ##p < 0.01, and ###p < 0.001 *vs.* scopolamine.

ROS levels is shown in Fig. 6B. Scopolamine showed increased ROS levels when compared with the control. However, animals treated with bulk quercetin, Q-ORMOSIL, and LF-Q-ORMOSIL groups showed decreased levels of ROS when compared with scopolamine. The data obtained were statistically significant. Furthermore, the effects of the nanoparticles on catalase levels revealed that the scopolamine group showed decreased catalase levels when compared with the control. However, the bulk quercetin, Q-ORMOSIL, and LF-Q-ORMOSIL treatment groups showed increased levels when compared with scopolamine. Comparing quercetin alone and Q-ORMOSIL, the group treated with LF-Q-ORMOSIL revealed a substantial difference in the levels of catalase (Fig. 6C). Likewise, the effect of nanoparticles on SOD levels is shown in Fig. 6D. Scopolamine showed decreased SOD levels when compared with the control. However, the quercetin, Q-ORMOSIL and LF-Q-ORMOSIL treatment groups showed increased levels of SOD when compared with scopolamine. When compared to the control group, the rats exposed to scopolamine had considerably lower GSH levels, as shown in Fig. 6E. When compared to the scopolamine group, the levels of GSH were significantly higher in the quercetin, Q-ORMOSIL, and LF-Q-ORMOSIL groups. The data obtained were statistically significant.

Effects of LF-Q-ORMOSIL on structural and histological alterations in scopolamine-induced neurotoxicity

Hematoxylin and eosin (HE) staining was used to identify histological alterations in the hippocampal region, as shown in Fig. 7. A light microscope was used to examine sections. The control group had normal, healthy normochromic neurons with well-defined cell bodies and no intercellular gaps (black arrow – normal pyramidal cell) (Fig. 7A). In the hippocampal region, the scopolamine-treated group showed marked and severe neuronal degeneration with perivascular edema, neuronophagia, pyknotic cells, and gliosis when compared to the control and treatment groups (Fig. 7B). On the other hand, the SCO + donepezil group showed mild neuronal degeneration and neuronophagia (Fig. 7C), while the SCO + QUER group showed moderate neuronal degeneration with neuronophagia and edema (the black arrow shows intercellular edema) (Fig. 7D). The SCO + Q-ORMOSIL group showed mild perivascular edema with mild congestion and neuronal degeneration (the black arrow shows edema and the blue arrow shows pyknotic cell) (Fig. 7E), and the SCO + LF-Q-ORMOSIL showed mild perivascular edema and minimal pyknosis (the black arrow shows mild edema, and the blue

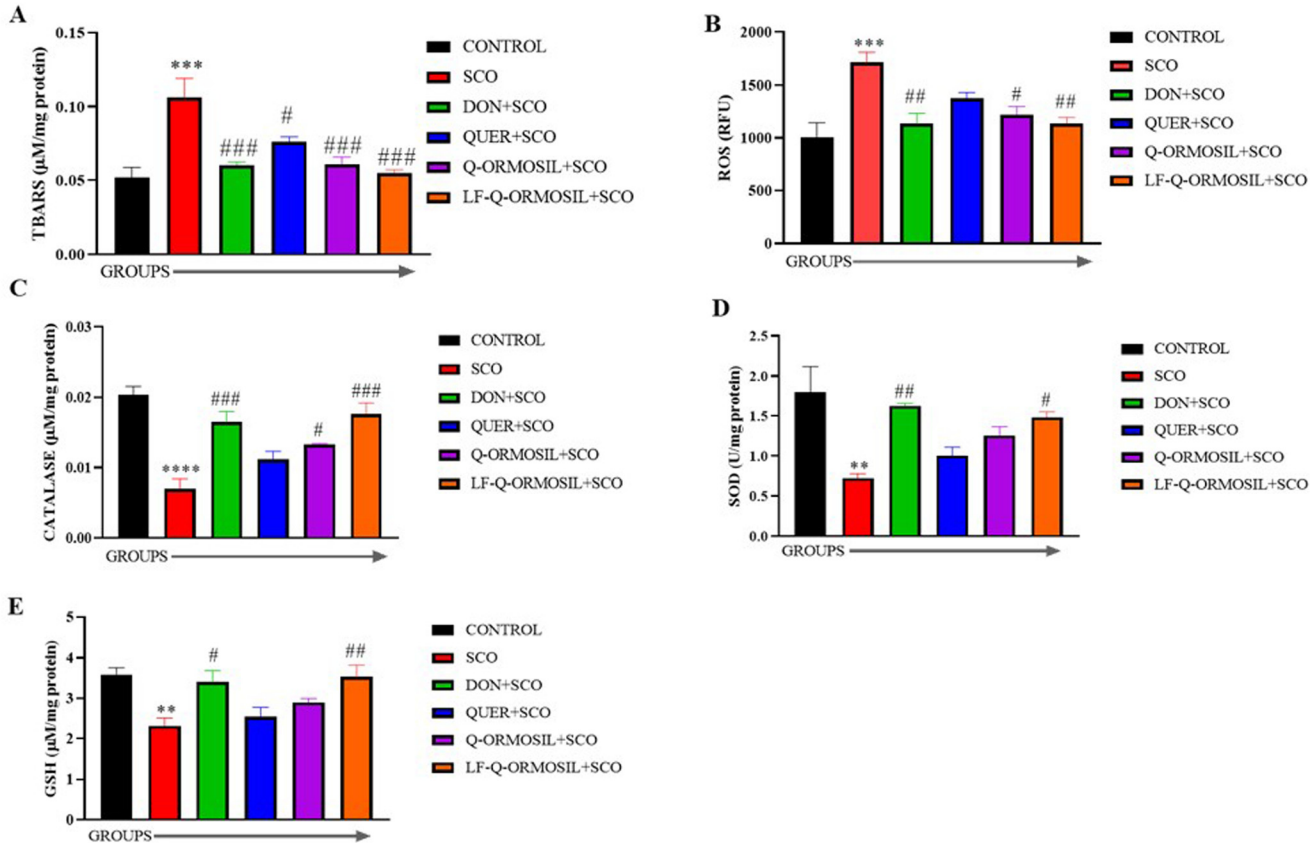

Fig. 6 Biochemical assessment: the anti-oxidant potential of LF-Q-ORMOSIL in comparison with other groups was assessed by (A) lipid peroxidation assay, (B) ROS scavenging properties, (C) catalase assay, (D) SOD assay, and (E) GSH assay. Data are represented as mean ± SEM. Statistical analysis is carried out by using one way ANOVA followed by Tukey's multiple comparison test, to estimate the antioxidant activity. The statistical significance was considered at *$p < 0.05$, **$p < 0.01$, ***$p < 0.001$, and ****$p < 0.0005$ *vs.* control; #$p < 0.05$, ##$p < 0.01$, ###$p < 0.001$, and ****$p < 0.0005$ *vs.* scopolamine.

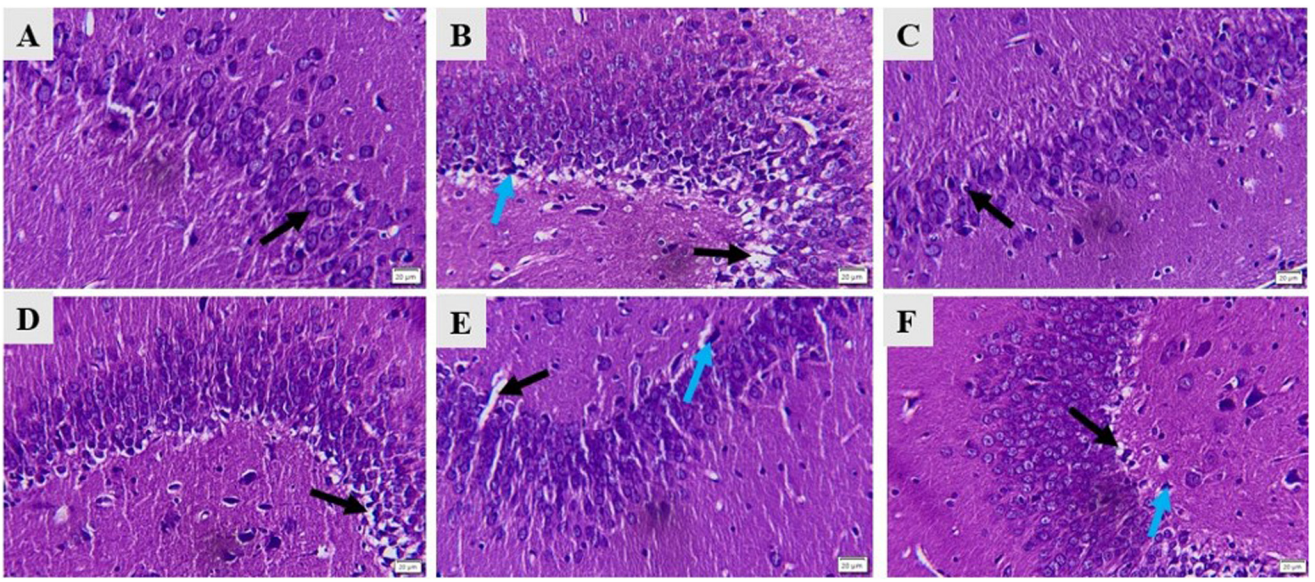

Fig. 7 Histological assessment: histopathology of the rat brain (hippocampus section) with H&E 40× and scale bar is 20 μm. (A) Control group, (B) SCO induced group, (C) SCO + donepezil group, (D) SCO + QUER group, (E) SCO + Q-ORMOSIL group, and (F) SCO + LF-Q-ORMOSIL.

arrow shows minimal pyknosis) with an overall improvement in neuronal score (Fig. 7F).

In vivo and *ex vivo* biodistribution patterns of free ICG and ICG loaded LF-Q-ORMOSIL at different time points

To investigate the accumulation of ORMOSIL nanoparticles in the body, the biodistribution pattern of nanoparticles was assessed by *in vivo* and *ex vivo* fluorescence imaging of rats. After intraperitoneal injection of free ICG and ICG-loaded ORMOSIL nanoparticles, the fluorescent signals were measured in the whole rat body. The results suggested that the free ICG signal started declining after 6 h post-injection in rats, and 24 h post injection, no signal in free ICG rats was detected. In contrast, in the ICG loaded ORMOSIL and lactoferrin conjugated nanoparticles, the signal started decreasing after 12 h. The FL intensity of LF coated nanoparticles was noticeable 24 h after, as shown in Fig. 8A, and the fluorescence intensity showed signals in the brain 3 h after injection which started to decrease after 12 h; this showed the accumulation of nanoparticles in the brain. To validate the brain delivery of LF-conjugated ORMOSIL, *ex vivo* imaging was done along with the brain and other major organs, and it was seen that the ICG loaded ORMOSIL nanoparticles showed the most abundant accumulation in the liver, and the signal also shows accumulation in the brain, kidneys, and testes (Fig. 8B). Better brain accumulation can be seen in the lactoferrin-conjugated ORMOSIL group (Fig. 8B).

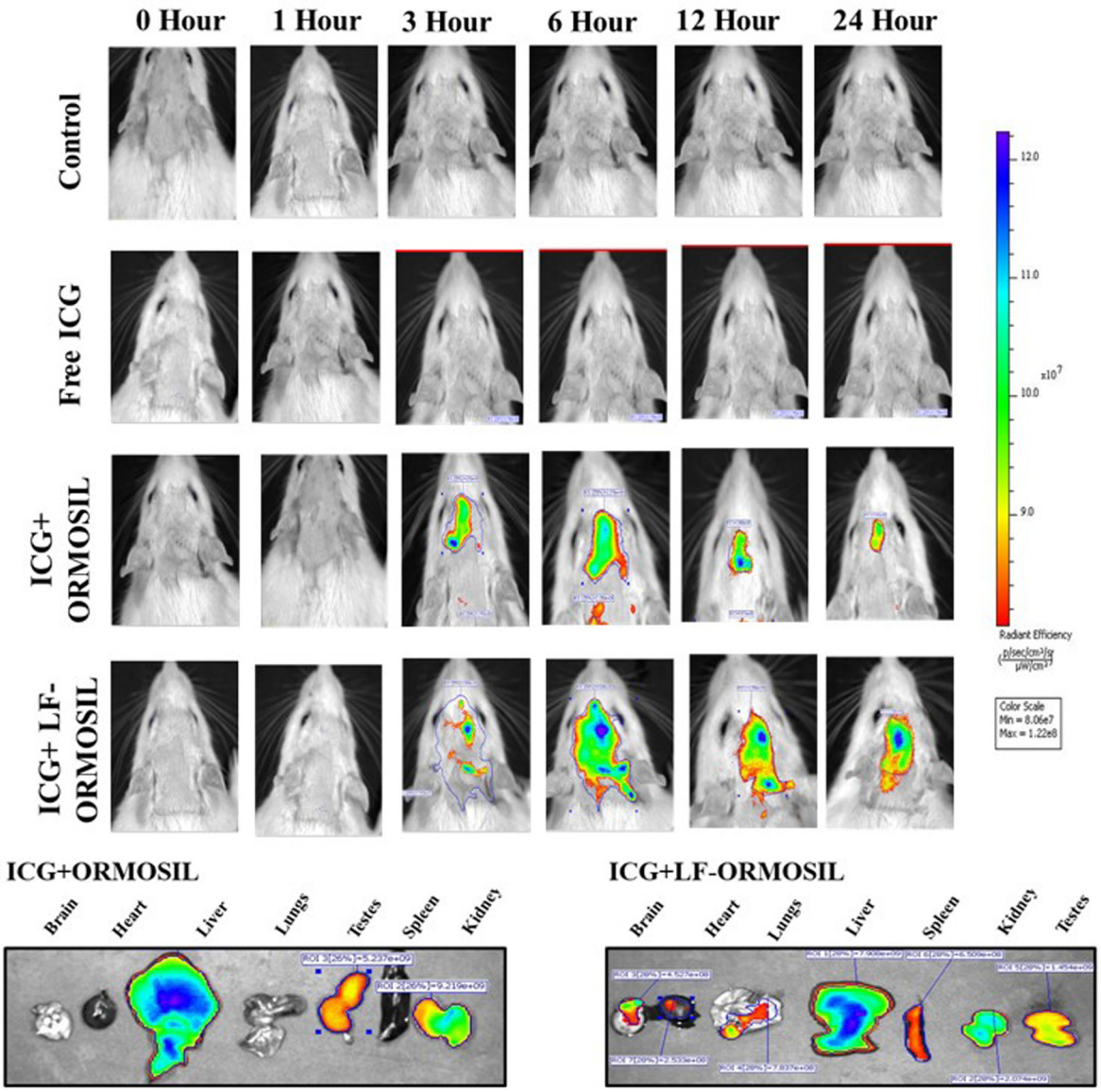

Fig. 8 Biodistribution assessment: (A) *in vivo* imaging of a rat and biodistribution after intraperitoneal injection with free ICG and ICG loaded ORMOSIL nanoparticles and ICG loaded LF-ORMOSIL nanoparticles at 0, 1, 3, 6, 12, and 24 hours; (B) fluorescence intensities in the major organs after injection with ICG loaded ORMOSIL nanoparticles and ICG loaded LF-ORMOSIL nanoparticles 24 hours post injection in a rat.

Discussion

Nanomedicine is a cutting-edge alternative to traditional drug delivery techniques and plays a significant role in therapeutics and targeted medication delivery. Increasingly, nanoparticles are used to treat various neurological conditions.[26] We developed monodisperse, spherical-targeted LF-Q-ORMOSIL nanoparticles for the current investigation to administer quercetin, a powerful antioxidant. Fig. 1 shows a schematic description of the development, characterization, and *in vivo* testing of nanoparticles. The effectiveness of LF coupled ORMOSIL nanoparticles against scopolamine-induced amnesia is reported in our current results. Using various drug carriers linked to the appropriate receptors on the cell surface, targeted drug delivery successfully achieves the selective medication delivery to targeted tissues, organs, and cells. To the synthesized silica nanoparticles, we added an organic group, amine, which gives them flexibility compared to the silica base alone and improves their stability in aqueous medium against flocculation/aggregation. A target-based moiety, lactoferrin (LF), is additionally readily conjugated on the organic arm of the surface of ORMOSIL nanoparticles. We therefore advise using this type of alteration in future research as it may allow for further manufacturing with additional diagnostic, therapeutic, or bio-targeting chemicals and make the nanoparticles suitable as "multimodal" nanoparticles. In our investigation, three different therapy regimens, quercetin alone, Q-ORMOSIL, and LF-Q-ORMOSIL nanoparticles, were used. Nanoparticles were developed to enhance quercetin's bioavailability and solubility in the system. According to the study, scopolamine-induced amnesia might be prevented more effectively by quercetin-loaded ORMOSIL nanoparticles than by quercetin alone. The data from this investigation, in particular different blood parameters, biochemical (including oxidative stress), and histological tests, confirm our view. The presence of quercetin in the nanoparticles was determined by UV-visible spectroscopy, which reveals that quercetin and quercetin-loaded nanoparticles have an absorbance peak at a wavelength of 368 nm. No peak at a wavelength of 368 nm was seen for void nanoparticles. It was proved that the drug has been successfully incorporated into the reverse micellar core of the ORMOSIL nanoparticles by the presence of the quercetin characteristic peak at 410 nm. To ascertain the existence of surface and functional groups as well as the interaction of the functional groups with the drug moiety, FT-IR spectroscopy was used. The peaks at 3375 cm^{-1}, 1362 cm^{-1}, and 2928 cm^{-1} were the typical quercetin peaks. However, these peaks were not seen in the case of Q-ORMOSIL nanoparticles, indicating that there had been some sort of interaction between quercetin and silica nanoparticles. This interaction caused the peaks to disappear, confirming the loading of quercetin within the nanoparticles. By using FTIR spectroscopy, the surface alteration of Q-ORMOSIL by LF was also confirmed. The amine group of the Q-ORMOSIL nanoparticle forms an amide bond with a carboxylic group of lactoferrin, which is activated by EDC and NHS, to create a stable product. The peak at 3334 cm^{-1}, which indicates NH_2 vibration with increased absorption, and the peak at 1640 cm^{-1}, which shows N–H bond production with a high intensity, served as confirmation. The effective conjugation of LF on the surface of Q-ORMOSIL and the encapsulation of quercetin in ORMOSIL nanoparticles are supported by all the observed peaks. SEM, TEM, and EDX were used to further characterize the synthesized nanoparticles. TEM is used to analyze the morphology, size, and shape of nanoparticles. According to the TEM image, quercetin nanoparticles were typically around 80 nm in size and had a monodisperse, spherical form. The monodisperse, spherical morphology of LF-Q-ORMOSIL nanoparticles (80 nm *via* TEM) enhances blood–brain barrier penetration, addressing a key limitation in neurological drug delivery.[27] This size range optimizes cellular uptake while minimizing clearance, explaining the superior *in vivo* efficacy. Furthermore, dynamic light scattering (DLS), was used to confirm the particle size distribution based on intensity. An average size of 103 nm was discovered. This measurement critically assesses the potential biological behavior of the nanoparticles. Nanoparticle size in the 100 nm range is particularly advantageous for drug delivery applications, as it enables prolonged circulation time, efficient tissue penetration, and enhanced cellular uptake. Studies have shown that nanoparticles within this size range enhance permeability and the retention effect, allowing for preferential accumulation in target tissues while minimizing rapid clearance by the kidneys or uptake by the reticuloendothelial system. Furthermore, DLS provides rapid, non-destructive assessment of nanoparticle dispersity and stability in solution, which are essential for ensuring reproducibility and efficacy in biological systems. Thus, the DLS results confirm the successful synthesis of monodisperse nanoparticles and underscore their suitability for effective drug delivery *in vivo*.[28]

We further confirmed that silica is present in the produced nanoparticles, through EDX investigation. The proportion of the drug that is successfully captured in the nanoparticle carriers is measured by the entrapment efficiency, which for quercetin-loaded nanoparticles was around 89%. Our findings showed that ORMOSIL nanoparticles are an effective means of trapping and delivering hydrophobic pharmaceuticals to a greater extent. The entrapment efficiency of quercetin within the ORMOSIL nanoparticles was found to be approximately 89%, indicating a highly effective encapsulation process. This high entrapment efficiency is particularly significant for hydrophobic drugs, which typically suffer from poor aqueous solubility and limited bioavailability when administered in their free form. The ORMOSIL matrix, with its tailored organic–inorganic hybrid structure, provides an optimal microenvironment for accommodating hydrophobic molecules, thereby reducing premature drug leakage and enhancing the stability of the encapsulated compound. Such a high level of drug loading not only maximizes the therapeutic payload delivered to target tissues but also minimizes the frequency and dosage of administration required to achieve therapeutic efficacy.[18] ORMOSIL also prevents drug degradation from the cytosolic environment by encasing a significant quantity of the drug. In

contrast, an *in vitro* release study indicates the amount of drug released over a specific period. The nanoparticles show a sustained release of quercetin over time at a physiological pH of 7.4 in phosphate buffer. It is further confirmed that the synthesized ORMOSIL nanoparticles contained quercetin inside their core and continuously released the drug because 82% of the drug is released from nanoparticles within 96 hours. Fig. 8 illustrates biodistribution analysis in *in vivo* imaging. Both ICG-loaded Q-ORMOSIL and LF-Q-ORMOSIL nanoparticle groups started showing signals in the rat brain after 3 hours, and the FL intensity in the ICG-loaded LF-Q-ORMOSIL group was present in the brain up to 24 hours, but not in the Q-ORMOSIL group, and no signal was detected in the free ICG receiving group. An early sign of oxidative stress is the measurement of the levels of antioxidant enzymes, TBARS, and ROS.[29] By scavenging free radicals, quercetin has been previously shown to reduce the quantity of reactive oxygen species.[30,31] A considerable reduction in ROS and TBARS levels was seen after treatment with quercetin, Q-ORMOSIL, and LF-Q-ORMOSIL (Fig. 6). Rats given Q-ORMOSIL and LF-Q-ORMOSIL showed a significant reduction in ROS and TBARS as well. On the other hand, treatment with LF-Q-ORMOSIL nanoparticles resulted in a more noticeable reduction, further demonstrating the effectiveness of the drug delivery method. Our findings also indicated a decline in the activities of several antioxidant enzymes, including SOD, CATALASE, and GSH. This restoration of endogenous antioxidant capacity further supports the protective role of nanoparticle-encapsulated quercetin against oxidative stress-induced cellular injury. By converting harmful superoxide radicals to H_2O_2 and oxygen molecules, SOD reduces stress. H_2O_2 is further changed into a water molecule by the catalase enzyme. Catalase, GSH, and SOD did not change significantly after quercetin treatment. Catalase, GSH, and SOD were all markedly increased after treatment with Q-ORMOSIL and LF-Q-ORMOSIL (Fig. 6). Compared to other treatment groups, the LF-Q-ORMOSIL nanoparticle treated group showed a more pronounced elevation of catalase, GSH, and SOD. Interestingly, when compared to the quercetin group, the LF-Q-ORMOSIL group has demonstrated a more pronounced inhibitory impact on the acetylcholinesterase enzyme. Our study's key finding implies that LF-Q-ORMOSIL nanoparticles have a more significant positive impact on animal health than bulk quercetin treatment. Notably, quercetin, a potent antioxidant, exhibited therapeutic efficacy at low concentrations when delivered *via* ORMOSIL nanocarriers. This enhanced effect is likely attributable to the high encapsulation efficiency and targeted delivery capabilities of ORMOSIL nanoparticles, which facilitate increased bioavailability and site-specific release of quercetin in tissues. The anti-oxidant drug quercetin appears to have therapeutic value at very low concentrations, according to our studies. This may be because ORMOSIL nano-carriers are highly effective at encapsulating drugs and delivering them just where they are needed. According to histopathological evidence, the group treated with scopolamine displayed severe neuronal degeneration, perivascular edema, neuronophagia, pyknotic cells, and gliosis. We observed a modest neuronal degeneration with minor pyknosis, and the group treated with quercetin-loaded ORMOSIL nanoparticles showed improvement. The natural hippocampal architecture was restored using targeted drug-loaded nanoparticles. We therefore conclude from the data that the use of quercetin-loaded ORMOSIL nanoparticles, as opposed to bulk quercetin, can more effectively alleviate scopolamine-induced amnesia.

Conclusion

Targeted nano-quercetin exhibits a strong neuroprotective impact compared to quercetin alone, against scopolamine-induced amnesia and significantly lowers the quercetin dosage by the reduction of oxidative stress. Additionally, we conclude that ORMOSIL nanoparticles improve quercetin's bioavailability by delivering the medication specifically to the brain. Due to the low bioavailability of quercetin, it is suggested that when the medicine is enclosed in a nanocarrier, LF-Q-ORMOSIL nanoparticles offer significantly better therapeutic efficacy in the prevention of scopolamine-induced amnesia than quercetin alone. Future clinical applications for human neurodegenerative diseases may be possible by this method of quercetin delivery in the form of nanoparticles.

Author contributions

The manuscript was written through the contributions of all authors. All authors have given approval to the final version of the manuscript.

Conflicts of interest

The authors declare that there are no competing interests.

Ethics approval and consent to participate

The use of animals in the study was approved by the IAEC.

Data availability

The data sets generated during and/or analyzed during the current study are available from the corresponding author on reasonable request.

Acknowledgements

The authors thank the CoE-NDDS, Department of Pharmaceuticals, Ministry of Chemical and Fertilizers, Government of India for their support. Communication No/NIPER-R/381.

References

1 S. Palle and P. Neerati, Cairo University Quercetin nanoparticles attenuates scopolamine induced spatial memory deficits and pathological damages in rats, *Bull. Fac. Pharm.*, 2017, **55**, 101–106.
2 J. Rajangam, Effect of Rosuvastatin on learning and memory in scopolamine induced amnesia in Mice, *Trends Med.*, 2018, **18**, 1–4.
3 D. A. El-Sherbiny, A. E. Khalifa, A. S. Attia and E. E.-D. S. Eldenshary, Hypericum perforatum extract demonstrates antioxidant properties against elevated rat brain oxidative status induced by amnestic dose of scopolamine, *Pharmacol. Biochem. Behav.*, 2003, **76**, 525–533.
4 I. Misane and S. O. J. N. Ögren, Selective 5-HT1A antagonists WAY 100635 and NAD-299 attenuate the impairment of passive avoidance caused by scopolamine in the rat, *Neuropsychopharmacology*, 2003, **28**, 253–264.
5 Z. Kerem, B.-A. Bravdo, O. Shoseyov and A. Tugendhaft, Rapid liquid chromatography–ultraviolet determination of organic acids and phenolic compounds in red wine and must, *J. Chromatogr.*, 2004, **1052**, 211–215.
6 C. Kanadaswami, L.-T. Lee, P.-P. H. Lee, J.-J. Hwang, F.-C. Ke, Y.-T. Huang and M.-T. Lee, The antitumor activities of flavonoids, *In Vivo*, 2005, **19**, 895–909.
7 A. W. Boots, G. R. Haenen and A. Bast, Health effects of quercetin: from antioxidant to nutraceutical, *Eur. J. Pharmacol.*, 2008, **585**, 325–337.
8 K. A. Khaled, Y. M. El-Sayed and B. M. Al-Hadiya, Disposition of the flavonoid quercetin in rats after single intravenous and oral doses, *Drug Dev. Ind. Pharm.*, 2003, **29**, 397–403.
9 R. Kumar, I. Roy, T. Y. Ohulchanskyy, L. N. Goswami, A. C. Bonoiu, E. J. Bergey, K. M. Tramposch, A. Maitra and P. N. Prasad, Covalently dye-linked, surface-controlled, and bioconjugated organically modified silica nanoparticles as targeted probes for optical imaging, *ACS Nano*, 2008, **2**, 449–456.
10 R. Huang, W. Ke, Y. Liu, C. Jiang and Y. Pei, The use of lactoferrin as a ligand for targeting the polyamidoamine-based gene delivery system to the brain, *Biomaterials*, 2008, **29**, 238–246.
11 Y. Song, D. Du, L. Li, J. Xu, P. Dutta and Y. Lin, In Vitro Study of Receptor-Mediated Silica Nanoparticles Delivery across Blood-Brain Barrier, *ACS Appl. Mater. Interfaces*, 2017, **9**, 20410–20416.
12 C. Fillebeen, L. Descamps, M.-P. Dehouck, L. Fenart, M. Benaïssa, G. Spik, R. Cecchelli and A. Pierce, Receptor-mediated transcytosis of lactoferrin through the blood-brain barrier, *J. Biol. Chem.*, 1999, **274**, 7011–7017.
13 R. Qiao, Q. Jia, S. Hüwel, R. Xia, T. Liu, F. Gao, H. J. Galla and M. Gao, Receptor-mediated delivery of magnetic nanoparticles across the blood-brain barrier, *ACS Nano*, 2012, **6**, 3304–3310.
14 R. Q. Huang, W. L. Ke, Y. H. Qu, J. H. Zhu, Y. Y. Pei and C. Jiang, Characterization of lactoferrin receptor in brain endothelial capillary cells and mouse brain, *J. Biomed. Sci.*, 2007, **14**, 121–128.
15 R. Huang, W. Ke, L. Han, Y. Liu, K. Shao, C. Jiang and Y. Pei, Lactoferrin-modified nanoparticles could mediate efficient gene delivery to the brain in vivo, *Brain Res. Bull.*, 2010, **81**, 600–604.
16 Y. A. Suzuki, V. Lopez and B. Lönnerdal, Mammalian lactoferrin receptors: structure and function, *Cell. Mol. Life Sci.*, 2005, **62**, 2560–2575.
17 Y. Kopaeva, A. B. Cherepov, I. Y. Zarayskaya and M. V. Nesterenko, Transport of Human Lactoferrin into Mouse Brain: Administration Routes and Distribution, *Bull. Exp. Biol. Med.*, 2019, **167**, 561–567.
18 S. Naqvi, H. Sharma and S. J. Flora, Lactobionic acid conjugated quercetin loaded organically modified silica nanoparticles mitigates cyclophosphamide induced hepatocytotoxicity, *Int. J. Nanomed.*, 2019, 8943–8959.
19 M. Ali, N. Mathur and S. V. Chandra, Effect of chronic cadmium exposure on locomotor behaviour of rats, *Indian J. Exp. Biol.*, 1990, 653–656.
20 M. S. Kim, D. Y. Lee, J. Lee, H. W. Kim, S. H. Sung, J. S. Han and W. K. Jeon, Terminalia chebula extract prevents scopolamine-induced amnesia via cholinergic modulation and anti-oxidative effects in mice, *BMC Complementary Altern. Med.*, 2018, **18**, 136.
21 D. Socci, K. Bjugstad, H. Jones, J. Pattisapu and G. W. Arendash, Evidence that oxidative stress is associated with the pathophysiology of inherited hydrocephalus in the H-Tx rat model, *Exp. Neurol.*, 1999, **155**, 109–117.
22 S. Naqvi, H. Sharma and S. J. Flora, Lactobionic acid conjugated quercetin loaded organically modified silica nanoparticles mitigates cyclophosphamide induced hepatocytotoxicity, *Int. J. Nanomed.*, 2019, **14**, 8943.
23 A. K. Sinha, Colorimetric assay of catalase, *Anal. Biochem.*, 1972, **47**, 389–394.
24 P. J. Hissin and R. Hilf, A fluorometric method for determination of oxidized and reduced glutathione in tissues, *Anal. Biochem.*, 1976, **74**, 214–226.
25 P. Kakkar, B. Das and P. Viswanathan, A modified spectrophotometric assay of superoxide dismutase, *Indian J. Biochem. Biophys.*, 1984, 130–132.
26 K. K. Jain, Role of nanotechnology in developing new therapies for diseases of the nervous system, *Nanomedicine*, 2006, **1**, 9–12.
27 M. M. Agwa and S. Sabra, Lactoferrin coated or conjugated nanomaterials as an active targeting approach in nanomedicine, *Int. J. Biol. Macromol.*, 2021, **167**, 1527–1543.
28 M. Kumar, P. Kulkarni, S. Liu, N. Chemuturi and D. K. Shah, Nanoparticle biodistribution coefficients: A quantitative approach for understanding the tissue distribution of nanoparticles, *Adv. Drug Delivery Rev.*, 2023, **194**, 114708.
29 J. M. Gutteridge, Lipid peroxidation and antioxidants as biomarkers of tissue damage, *Clin. Chem.*, 1995, **41**, 1819–1828.
30 K. E. Heim, A. R. Tagliaferro and D. J. Bobilya, Flavonoid antioxidants: chemistry, metabolism and structure-activity relationships, *J. Nutr. Biochem.*, 2002, **13**, 572–584.
31 M. Erden Inal and A. Kahraman, The protective effect of flavonol quercetin against ultraviolet A-induced oxidative stress in rats, *Toxicology*, 2000, **154**, 21–29.